

Lipid microbubbles as a vehicle for targeted drug delivery using focused ultrasound-induced blood–brain barrier opening

Carlos Sierra¹, Camilo Acosta¹, Cherry Chen¹, Shih-Ying Wu¹, Maria E Karakatsani¹, Manuel Bernal² and Elisa E Konofagou^{1,3}

Abstract

Focused ultrasound in conjunction with lipid microbubbles has fully demonstrated its ability to induce non-invasive, transient, and reversible blood–brain barrier opening. This study was aimed at testing the feasibility of our lipid-coated microbubbles as a vector for targeted drug delivery in the treatment of central nervous system diseases. These microbubbles were labeled with the fluorophore 5-dodecanoylaminofluorescein. Focused ultrasound targeted mouse brains *in vivo* in the presence of these microbubbles for trans-blood–brain barrier delivery of 5-dodecanoylaminofluorescein. This new approach, compared to previously studies of our group, where fluorescently labeled dextrans and microbubbles were co-administered, represents an appreciable improvement in safety outcome and targeted drug delivery. This novel technique allows the delivery of 5-dodecanoylaminofluorescein at the region of interest unlike the alternative of systemic exposure. 5-dodecanoylaminofluorescein delivery was assessed by *ex vivo* fluorescence imaging and by *in vivo* transcranial passive cavitation detection. Stable and inertial cavitation doses were quantified. The cavitation dose thresholds for estimating, *a priori*, successful targeted drug delivery were, for the first time, identified with inertial cavitation were concluded to be necessary for successful delivery. The findings presented herein indicate the feasibility and safety of the proposed microbubble-based targeted drug delivery and that, if successful, can be predicted by cavitation detection *in vivo*.

Keywords

Blood–brain barrier, microscopy, MRI, targeted drug delivery, ultrasound

Received 20 January 2016; Revised 26 April 2016; Accepted 2 May 2016

Introduction

Focused ultrasound (FUS)-induced blood–brain barrier BBB opening is currently the sole technique to achieve noninvasive, transient, and localized drug delivery to the brain. This technique allows localized transport of both large and small molecules to the desired brain region by increasing the permeability of the BBB locally. The main function of the BBB is to eliminate toxic substances before entering the brain parenchyma. However, it recognizes most therapeutic agents ≥ 400 Da as foreign and blocks their delivery.¹ Many strategies have been used to overcome this key limitation, such as intracranial injection,² disruption by mannitol,³ gene therapy,⁴ and endogenous transport mechanisms.⁵ FUS in the presence of microbubbles remains the only non-invasive, transient, localized, and reversible way to

open the BBB.^{6–9} Its clinical utility has been shown to be an effective treatment for, e.g. the early onset of Alzheimer's, Huntington's and Parkinson's^{12–14} diseases, brain tumors,^{15–19} and against cerebral ischemia/reperfusion.²⁰

¹Department of Biomedical Engineering, Ultrasound and Elasticity Imaging Laboratory, Columbia University, New York, NY, USA

²Department of Microbiology and Immunology, Columbia University, New York, NY, USA

³Department of Radiology, Columbia University, New York, NY, USA

Corresponding author:

Elisa E Konofagou, Department of Biomedical Engineering, Columbia University, 351 Engineering Terrace, Mail Code 8904, 1210 Amsterdam Avenue, New York, NY 10027, USA.
Email: ek2191@columbia.edu

Our group has reported the use of this technique in mice^{12–14,21–30} and non-human primates (NHP),^{31–34} but in the cases where molecules of interest were administered, they were typically co-administered with microbubbles,^{13,14,28,29,35} allowing them to reach not only the brain, but also other organs through systemic circulation. Drug attachment onto the lipid shell diminishes this safety concern and introduces fewer potential side-effects to other organs. Therefore, this study aimed at the use of our in-house manufactured lipid-coated microbubbles as carriers for drug transportation and targeted delivery.

Ultrasound-stimulated microbubbles, containing the molecule of interest attached to the lipid shell, have been widely demonstrated as a method for localized drug delivery.^{36–38} There are two general methods for generating this kind of microbubbles;³⁹ through biotin-avidin linking or a direct covalent bond. Biotin-avidin linkage is a straightforward technique, in which a biotinylated ligand is coupled to a biotinylated microbubble via an avidin bridge. Although biotin-avidin linkage is useful in proof-of-concept and preclinical targeting studies, its immunogenicity precludes it from translation to humans. For this reason, the covalent attachment of the drug to the shell was deemed more desirable for our purposes.

Loaded microbubbles through covalent bond were used as vectors for localized drug delivery into the brain.^{16,19,40} Huang et al.⁴⁰ were able to achieve targeted gene delivery using FUS and lipid microbubbles loaded with DNA plasmids using the layer-by-layer assembly technique with the help of poly-L-lysine.⁴¹ Ting et al.¹⁶ demonstrated targeted drug delivery for brain glioma treatment after craniotomy in rats using lipid microbubbles loaded with chemotherapeutic agents (1,3-bis(2-chloroethyl)-1-nitrosourea). This agent, due to its hydrophobicity, is attached, as our fluorophore 5-dodecanoylaminofluorescein (C-12), to the phospholipid shell by electrostatic and hydrophobic interactions. The safety of these methods was not reported and they did not define physical parameters, which might assure successful delivery in vivo.

Based on previously reported in-house methods to prepare monodisperse (4–5 μm) microbubbles, we developed a new type of lipid-coated microbubbles for the purpose of this study. They were designed to contain the same lipid shell composition and gas core as in our previous studies,^{14,23,25,28,32–34,42–44} but converted to also elicit fluorescence through covalent binding of C-12 onto their shell. When FUS is applied to these microbubbles, they oscillate or cavitate. When cavitation occurs in the cerebral vasculature, it can induce localized BBB opening.^{45,46} Depending on the acoustic pressure, microbubbles present two types of cavitation. At relative low pressures, they exhibit

stable cavitation (SC) or nonlinear volumetric oscillation,⁴⁷ resulting in emissions of harmonics, subharmonics (not evaluated in this study), and ultraharmonics without microbubbles destruction. Meanwhile, at high pressures, the amplitude of oscillation increases and the bubbles can enter the inertial cavitation (IC) regime. IC, characterized by broadband emissions, refers to violent bubble oscillation leading to bubble collapse.⁴⁸

During SC, microbubbles can induce shear forces on the endothelium, which might lead to an increase in transcellular permeability without causing any vascular damage in rabbits,⁷ rodents,^{6,49} and NHP,³³ and therefore safely opening the BBB but, most likely, not delivering the C-12 due to the strong chemical bond between the C-12 and the lipid shell. In the regime of IC, however, the microbubbles can suddenly collapse and, therefore, there is no lipid shell to retain the C-12 attached to the microbubbles, allowing it to flow through the blood-pool and its delivery to the brain. IC has been shown to be associated with microdamage to the cerebral vessels.^{24,50} For this reason histological observations of the brains were performed for safety evaluation at two different time-points: 2 h and one week after sonication in order to detect any damage and, if so, to assess the reversibility of the damage over time.

During FUS sonication, in the presence of fluorescent microbubbles, acoustic emissions from oscillating microbubbles, stable cavitation dose from harmonics (SCD_h) and ultraharmonics (SCD_u), and inertial cavitation dose (ICD) were quantified in vivo by a transcranial passive cavitation detector (PCD). Approximately 2 h later, the mice were sacrificed to acquire fluorescence images of the mouse brains in order to evaluate the delivery of C-12 to the sonicated area. Both in vivo and ex vivo methods were compared in order to define, for the first time, cavitation dose thresholds, by which we may guarantee the success of the targeted C-12 delivery.

Hence, the main objective of this study was to evaluate the feasibility and the safety of our in-house manufactured, size-selected microbubbles as agents for targeted drug delivery, i.e. for carrying and delivering the compound to the region of BBB opening.

Materials and methods

The animal experiments have been reported in compliance with the Animal Research: Reporting in Vivo Experiments (ARRIVE) guidelines.

Synthesis of fluorescent microbubbles

The fluorescent microbubbles were manufactured based on our previously published protocol for in-house

and size-isolated lipid-coated microbubbles⁴² (Supplementary methods).

Briefly, they were formulated by dissolving 90% mol 1,2-distearoyl-sn-glycero-3-phosphocoline (DSPC) and 10% mol 1,2-distearoyl-sn-glycero-3-phosphoethanolamine-N-[methoxy(polyethylene glycol)2000] (DSPE-PEG2000) (Avanti Polar Lipids, Alabaster, AL) in a solution consisting of phosphate-buffered saline (PBS) 1×/glycerol (10% volume)/propylene glycol (10% volume). After dissolving, the gas core, perfluorobutane (PFB) at 99% wt. purity (FluoroMed, Round Rock, TX), was introduced in order to activate the microbubbles. Immediately after activation, the 4–5 μm microbubbles were isolated and their concentration and size distribution were measured.

The microbubbles were converted into fluorescent by the addition of the lipophilic fluorescein probe, C-12 (Life technologies, Eugene, OR) (molecular weight 529.63 g/mol, maximum emission and excitation wavelengths 497 ± 3 and 518 ± 4 nm, respectively) using a post-labeling technique. C-12 contains a C₁₂ alkyl chain (Figure 1(a)) that will bind to membranes with the fluorophore at the aqueous interface and the alkyl

tail protruding into the lipid interior (Figure 1(b)). C-12 was dissolved in pure ethanol at a concentration of 10 mM and put in direct contact with the microbubbles. Due to its amphiphilic nature, direct contact with the C-12 solution led to microbubbles binding to it. To allow the diffusion of C-12 to all the bubbles, the 1-mL syringe containing the suspension of microbubbles plus C-12 was incubated during 2 h at room temperature while it was rotating at 40 r/min. The size distribution and concentration of the microbubbles after making them fluorescent were determined again with the Coulter Counter Multisizer III. Figure 1(c) illustrates the appearance of the fluorescent microbubbles. It is clear that all the fluorescence is concentrated on the lipid shell.

Preparation of animals

All experiments were performed in strict accordance with the National Institutes of Health Guidelines for animal research; all animal procedures for these experiments were reviewed and approved by the Institutional Care and Use Committee of the Columbia University.

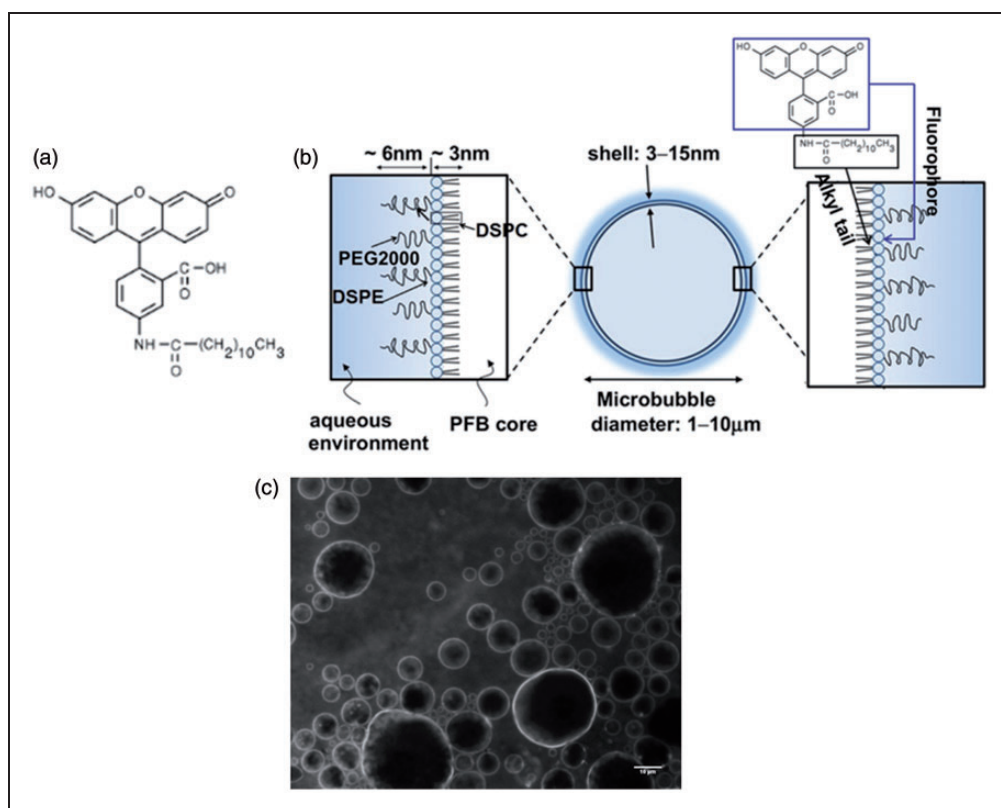


Figure 1. (a) Molecular structure of 5-dodecanoylamino fluorescein (C-12). (b) Cartoon showing how the C-12 alkyl tail protrudes into the microbubble lipid shell converting the microbubble into a fluorescent drug carrier. (c) Epi-fluorescence image of a fluorescent microbubble sample. C-12 did not enter the core of the microbubbles; all the fluorescence is located at the lipid shell. The scale bar corresponds to 10 μm.

Table 1. Summary of experimental groups, BBB opening and fluorescence delivery quantification results.

Group	Pressure (kPa)	Successful BBB opening	Successful delivery	Fluorescence enhancement (A.U.)	p Value (if fluorescence enhancement > 0)	Time survived
1	450	4/4	0/4	0	–	2 h
2	600	15/15	3/9	4.63 ± 2.58	0.02	2 h
3	750	6/6	3/5	8.99 ± 6.85	0.04	2 h
4 (control)	450, 600, 750 ^a	6/6	0/4	0	–	2 h
5	600	5/5	n/a	n/a	n/a	1 week
6	750	7/7	n/a	n/a	n/a	1 week
7	750	4/4	n/a	n/a	n/a	2 weeks

BBB: blood–brain barrier. ^aTwo mice at each pressure

A total of 47 male mice (C57BL/6, Harlan, Indianapolis, IN) (age: 3–4 months old, weight: 20–25 g) were used in this study. The animals were divided into seven cohorts depending on the applied acoustic pressure and time of sacrifice (Table 1). Randomization had not been performed because all the mice were males from the same strain with similar age and weight.

All the mice were handled as in previous studies conducted by our group^{21,27} (Supplementary methods).

In vivo experimental procedure and MRI

The experimental FUS setup, as shown in Figure 2(a), was used as previously described^{24,29} (Supplementary methods).

The targeting procedure was carried out with a grid system to locate the sutures of the skull; the procedure has been described in great detail elsewhere.^{6,51} Briefly, the FUS focus was placed 3 mm below the skull and 18% attenuation was accounted for acoustic pressure loss through the skull.¹⁰

In this study, a pulsed FUS (pulse length 6.56 ms; pulse repetition frequency 5 Hz; duration 5 min) beam at acoustic pressures between 450 and 750 kPa was targeted transcranially to the left caudate-putamen (Cau-Pu), while the right side served as a control. Hence, each animal served as its own control, thereby reducing the variability caused by physiologic differences among animals.

Prior to fluorescent microbubbles administration, a 30-s sonication using the same acoustic parameters described above was applied in order to measure the baseline background signal needed in the acoustic emission analysis. The injected microbubbles were freshly diluted before each injection. A bolus of 50 μ l diluted fluorescent microbubbles in saline solution (8×10^8 microbubbles/ml) was injected intravenously through the tail vein immediately before sonication (Figure 2(b)). The microbubbles reached the targeted region in under 15 s (time window between the injection

of the fluorescent microbubbles and the beginning of sonication) according to the spectrograms obtained from the PCD data (Supplementary Figure 1). Here, comparing the spectrogram corresponding to the control (Supplementary Figure 1(a), FUS without microbubbles), where only the reflected signal (1.5 MHz) and the effect from the skull (3.0 MHz, the second harmonics) are observed, with the spectrogram corresponding to the first FUS pulse after injecting the microbubbles (Supplementary Figure 1(b)). The harmonic, ultraharmonic, and broad-band emissions associated with the oscillation of the microbubbles are present since the beginning of sonication. One control cohort was used, where ultrasound was applied at 450, 600, and 750 kPa, and C-12 (2 μ l at 10 mM) dissolved in 50 μ l of saline solution (final concentration of C-12 0.4 mM) was co-administered 30 s after in the presence of non-fluorescent microbubbles to serve as the basis for comparison in the fluorescent imaging analysis (Supplementary methods).

After sonication, post-contrast T₁-weighted (T₁-w) MRI was conducted in order to confirm the BBB opening by a 9.4-T MRI system (Bruker Medical, Boston, MA) (Supplementary methods).

Four additional mice sonicated at 750 kPa were survived two weeks in order to analyze when the BBB integrity was restored. In these mice, T₁-w post-Gd injection MRI was repeated on a daily basis starting from the day of sonication and lasting up to 14 days after sonication.

In some mice, T₂-weighted (T₂-w) MRI was acquired for safety evaluation (presence or absence of edema at the sonicated region) (Supplementary methods).

The same four mice used for studying the closing timeline of the BBB were also imaged with T₂-w MRI on a daily basis to determine edema progression.

The mice were sacrificed at different time-points to assess the fluorescence delivery and microscopic damage 2 h after sonication in order to evaluate the

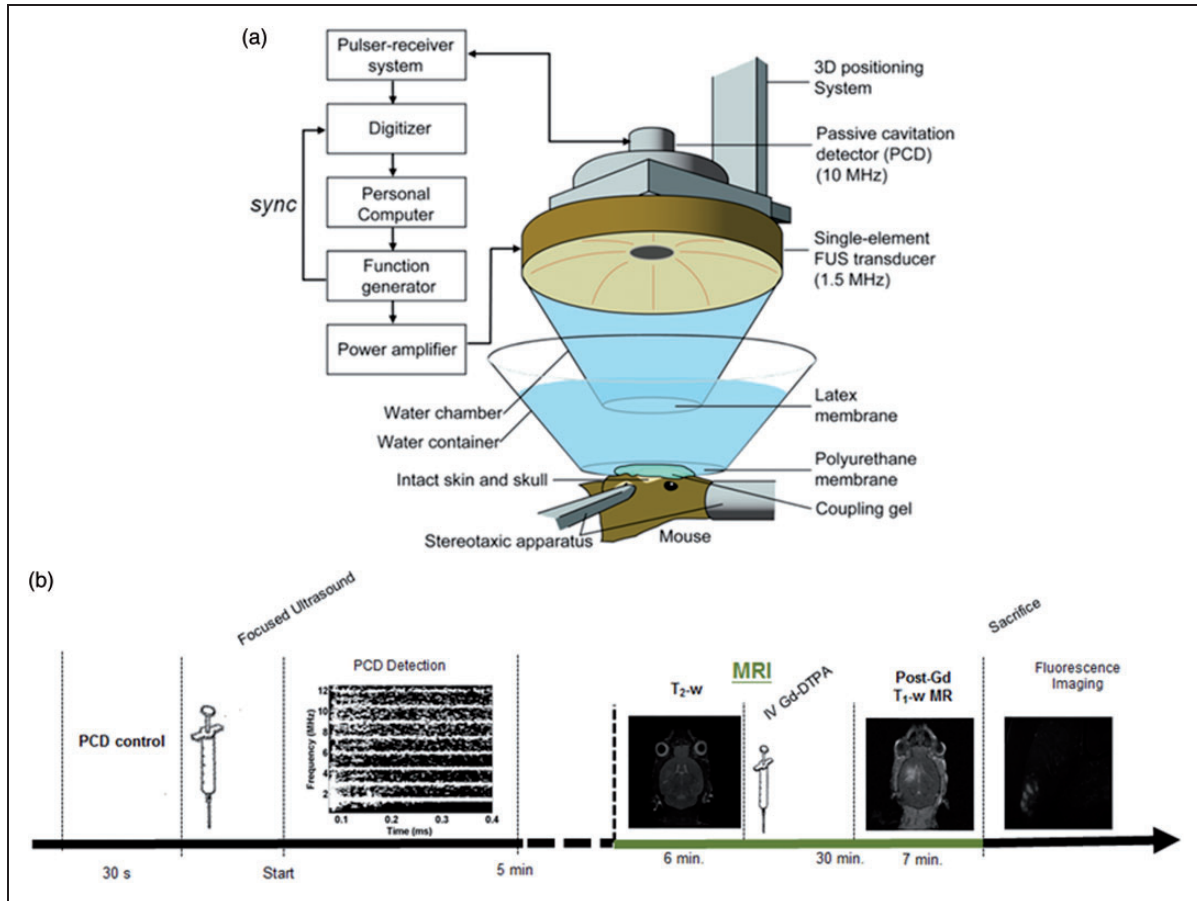


Figure 2. (a) Experimental setup of in vivo FUS-induced BBB opening and transcranial cavitation detection. (b) Illustration of the experimental timeline. Sonication started ≈ 15 s after the injection of the fluorescent microbubbles. During the 5-min sonication, transcranial PCD was performed. The mice underwent T₂-w and T₁-w imaging 20 min after finishing the sonication. Two hours after fluorescent microbubble injection, they were transcardially perfused, the brains fixed and then horizontally sectioned for fluorescence imaging.

fluorescence delivery and short-term microscopic damage. This time-point was selected to enable the detached C-12 to diffuse into the brain parenchyma in the region of BBB opening; and one week to evaluate long-term microscopic damage and potential microglial activation (Supplementary methods).

Cavitation emission quantification

The acoustic emissions from the ultrasound-activated fluorescent microbubbles were detected and quantified, as described previously,^{33,35,44} using stable cavitation dose (SCD) and ICD to assess the two types of cavitation activity (Supplementary methods).

Fluorescence imaging analysis

The efficiency of the C-12 delivery was assessed based on the quantification of the fluorescence enhancement in the targeted regions.

A spinning-disk confocal (CSU10; Yokogawa, Tokyo, Japan), inverted microscope (Eclipse Ti; Nikon, Melville, NY) with an electron-multiplying charge-coupled device camera (Hamamatsu Photonics, Hamamatsu, Japan) and 100 \times /1.4 numerical aperture objective with a 1.5 \times magnifier was used for image acquisitions of the fluorescent microbubbles. Image acquisition was performed using Micromanager 1.4.⁵²

Epi-fluorescence images of the brain sections were captured using an Olympus DP30BW digital camera mounted on an upright Olympus BX61 microscope. The fluorescence enhancement was quantified in a similar manner following the previously published protocol⁵³ (Supplementary methods).

In order to evaluate the spatial location of the fluorescence distribution in the brains, the slides were mounted with ProLong[®] Diamond Antifade Mountant (Thermo Fisher, Waltham, MA) with the nuclear marker DAPI.

Histological analysis

Whole brain histological examinations were performed using H&E stain for general histology (Supplementary methods).

Thirteen mice were used for histological observations: Four mice sacrificed 2 h after sonication at 600 (n=2) and 750 kPa (n=2); nine additional mice survived during one week to evaluate the length and severity of the damage, it means, for intensity quantification of the damage and its recovery.

Both the sonicated and nonsonicated sides were evaluated.

Immunohistochemistry

In order to detect potential microglial activation as consequence of the treatment with FUS, Iba1 bright-field immunohistochemistry was performed in three mice sonicated at 750 kPa and survived for one week (Supplementary methods).

Statistical analysis

Statistical analysis was performed using GraphPad Prism (Version 5.01, La Jolla, CA). For each study group, the mean \pm standard deviation of the fluorescence enhancement was calculated. Successful C-12 delivery was concluded if the fluorescence enhancement was statistically higher than zero (one-tailed, one-sample Student's t-test). Unpaired two-tailed Student's t-tests were used to determine whether the ICD, SCD_h, and SCD_u, at 30 s, 1 min and 5 min, were

significantly different between the cases, where C-12 was delivered and the cases where it was not. A p -value < 0.05 was considered to represent a significant difference in the analysis.

Results

Fluorescent microbubble generation

The size distribution of microbubbles before and after tagging with fluorescence is showed in Figure 3. After rendering them fluorescent, the mean size decreased by approximately 12% (from $4.56 \pm 0.76 \mu\text{m}$ to $4.00 \pm 1.13 \mu\text{m}$) while maintaining monodisperse distribution.

However, while non-fluorescent microbubbles are stable for, at least, three days, fluorescent microbubbles become quickly unstable in a matter of hours (data not shown) and they had to be used on the same day of the preparation.

BBB opening and targeted fluorophore delivery

Table 1 summarizes all the results obtained in this study. The BBB opening was revealed by post-Gd T₁-w MRI (Figure 4(a) to (c)), while fluorescence delivery was assessed by epi-fluorescence microscopy (Figure 4(d) to (e)). Not all the mouse brains were imaged by fluorescence microscopy since some of them were used for H&E staining, gross pathology (images not shown), and Iba1 immunohistochemistry in order to evaluate the safety of our method. In all

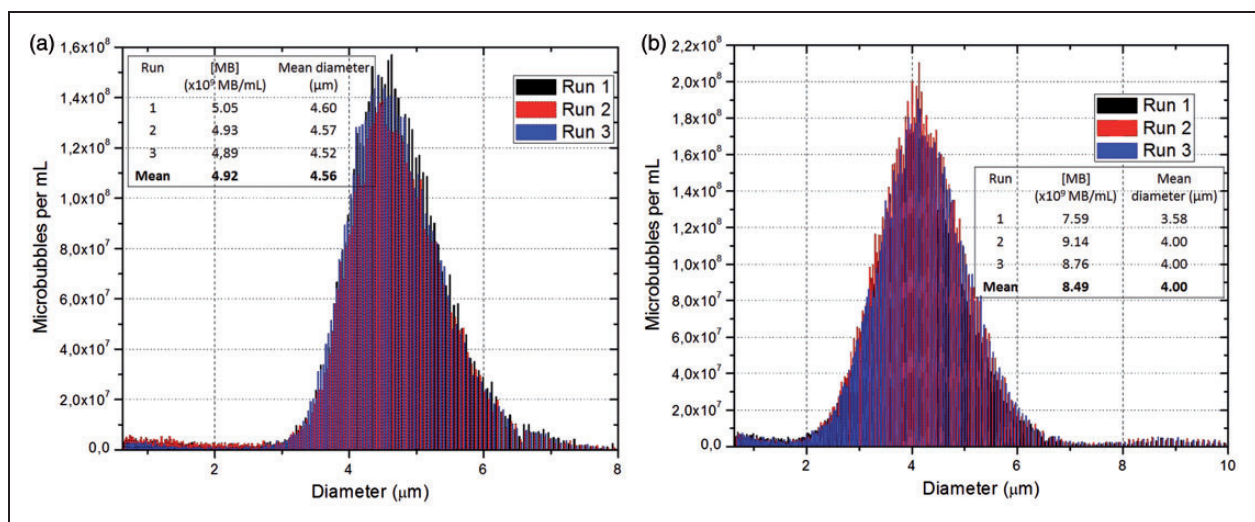


Figure 3. Representative size distributions of lipid monodisperse microbubbles before (a) and after (b) converting them into fluorescent microbubbles. Both distributions were measured by Coulter Multisizer III. The average number-weighted mean (averaged over three vials) and (\pm) standard deviations were $4.56 \pm 0.76 \mu\text{m}$ and $4.00 \pm 1.13 \mu\text{m}$, respectively (size decrease $\approx 12\%$). The fluorescent microbubbles were diluted to an 8×10^8 microbubbles/ml concentration before injecting.

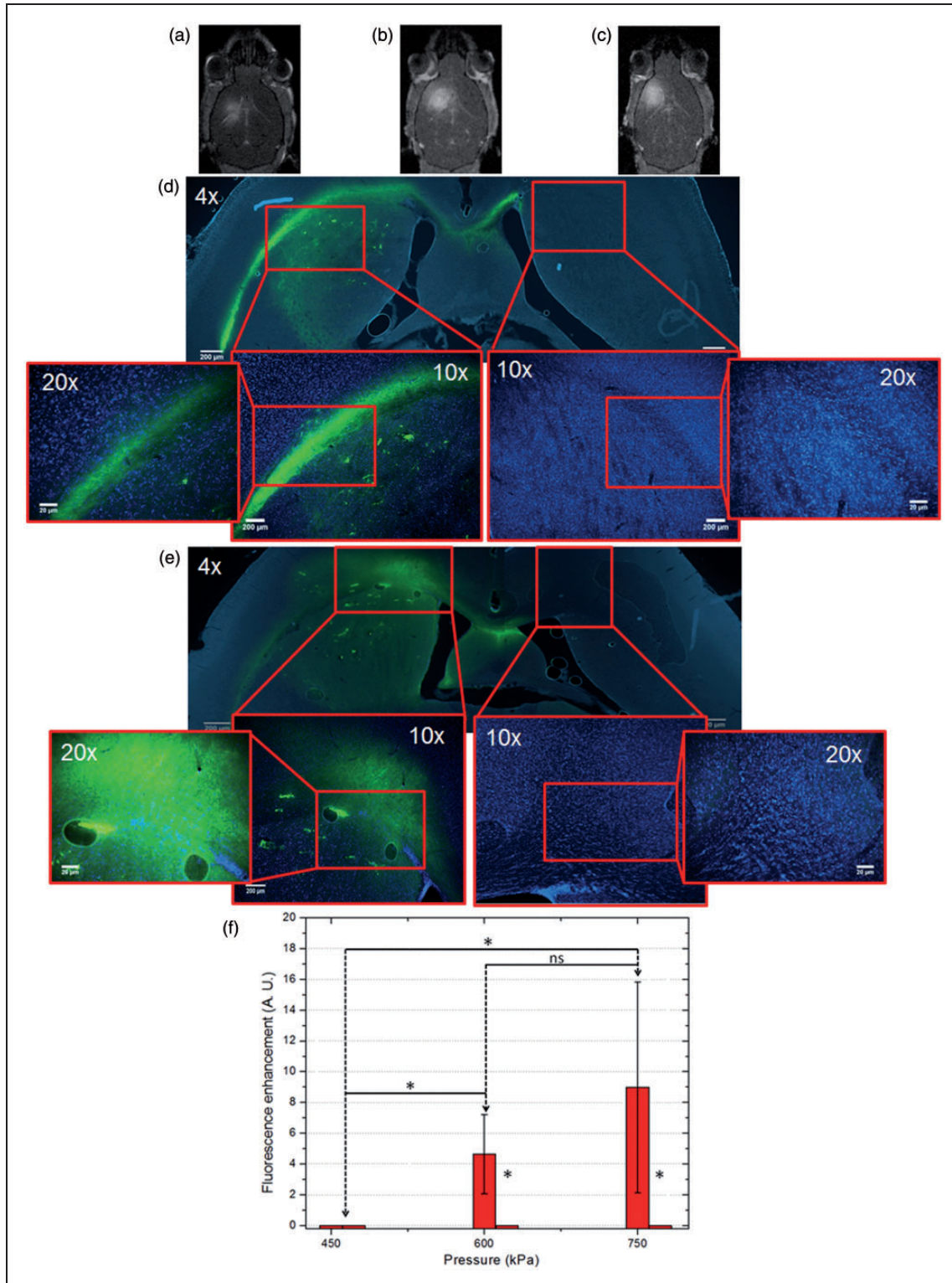


Figure 4. BBB opening and fluorescence delivery detection in the sonicated left Cau-Pu: Post-contrast-enhanced T1-w MRI showing BBB opening at acoustic pressures (a) 450 kPa, (b) 600 kPa, and (c) 750 kPa. Epi-fluorescence images of horizontal sections of two mouse brains sonicated at (d) 600 kPa and (e) 750 kPa. Fluorescence enhancement in the sonicated area was observed with respect to the contralateral unsonicated side. The boxed regions in areas at zoom 4 × are further zoomed in at 10 ×, while the boxed regions at zoom 10 × are zoomed in at 20 ×. Scale bars represent 200 μm at 4 × and 10 ×, and 20 μm at 20 ×. Brain sections showed in (d) and (e) were also stained with DAPI (blue) in order to reflect the spatial location of the fluorescence distribution (green). (f) Comparing the sonicated with the contralateral unsonicated region, fluorescence enhancement is observed. Significant C-12 delivery was observed at pressures higher than 450 kPa, but no differences were found between 600 kPa and 750 kPa. All numbers are reported as mean ± sd; *: $p < 0.05$.

cases, fluorescence delivery was achieved at the site of the BBB opening, co-localized with fluorescence enhancement regions.

Figure 4(d) and (e) shows representative fluorescence images obtained from mouse brains sonicated at their left Cau-Pu at pressures of 600 and 750 kPa, respectively (at 450 kPa fluorescence was not observed in any case). Images of the left Cau-Pu exhibited successful delivery of C-12 in the sonicated region, while images of the right Cau-Pu depict the contralateral (unsonicated) side, where fluorescence enhancement was never observed. At 600 kPa, the BBB was opened in all the cases and the C-12 was successfully delivered in three out of the nine cases, while at 750 kPa, the BBB was also opened in all the cases and FUS treatment resulted in a successful delivery of C-12 throughout the left Cau-Pu in three out of the five cases. In order to reflect correctly, the spatial location of C-12 throughout the sonicated region the nuclear marker DAPI was added to the slices of interest.

Therefore, the likelihood of a successful delivery in the sonicated region increases with the FUS pressure. Under the control conditions (450, 600, and 750 kPa with co-administration of non-fluorescent microbubbles and free C-12) no mouse showed significant fluorescent enhancement despite achieving 100% opening efficiency. There was no statistically significant difference in fluorescence enhancement between the 600 and 750 kPa ($p=0.36$) cases, but the findings were statistically significant when comparing 600 and 750 kPa against the 450 kPa and control cases (Figure 4(f)).

Microbubble cavitation emissions

In Figure 5, two cases with typical cavitation activities (ICD, SCD_u , and SCD_h) are shown: a case where the C-12 was successfully delivered (Figure 5(a)) and a case where it was not delivered (Figure 5(b)).

ICD, SCD_u , and SCD_h were calculated at three different time-points (30 s, 1 min, and 5 min) in order to establish thresholds that could explain why the C-12 delivery was not successful in all cases. Figure 5(c) to (e) shows the comparison among the ICD at (c) 30 s, (d) 1 min, and (e) 5 min. For 30 s and 1 min, the quantified ICD showed a significant increase between the cases where the fluorophore was successfully and unsuccessfully delivered to the target area. However, no statistical difference was determined at 5 min. Figure 5(f) to (h) shows the equivalent case for the SCD_u at (f) 30 s, (g) 1 min and (h) 5 min. Similar to ICD, SCD_u showed significant increase between the cases where C-12 was successfully and unsuccessfully delivered to the target area for 30 s and 1 min. No statistical difference was observed at 5 min. Figure 5(i) to (k) depicts smaller

findings for the SCD_h at (i) 30 s, (j) 1 min, and (k) 5 min. SCD_h only showed significant increase between the cases where C-12 was successfully and unsuccessfully delivered to the targeted area for 30 s. No statistical difference was observed at 1 and 5 min.

According to the results shown in Figure 5, ICD, SCD_u , and SCD_h thresholds have been established (Supplementary Table 1). These thresholds were defined as two times the standard deviation above the mean cavitation dose of the non-fluorescent delivery. Applying higher cavitation doses than these thresholds may indicate a higher probability that C-12 would be delivered to the targeted (sonicated) region.

Safety

In order to evaluate the safety of this study, i.e. potential edema, possible erythrocyte extravasations, dark or necrotic neurons, gross hemorrhage and/or microvacuolations tissue, BBB opening closing time, and likely microglial activation were evaluated by T_2 -w MRI (edema), H&E stain (damage), T_1 -w MRI (BBB closing), and Iba-1 immunohistochemistry (microglial activation) in the sonicated brains.

In some mice sacrificed about 2 h after sonication, T_2 -w images were acquired 20 min after sonication and no edema was observed in most of the cases (data not shown), but in mice survived for one week after sonication, T_2 -w was repeated and edema was detected in all of them at 600 (Figure 6(a)) and 750 kPa (Figure 6(b)). In order to check whether the edema is restored, four mice were sonicated at 750 kPa and survived for two weeks. These mice were scanned on a daily basis to determinate the temporal extension of the edema. It was observed that in three out of the four cases, edema was repaired between days 3 and 4 (Supplementary Figure 2(b)), while in the other mice the edema remained after two weeks.

These four mice were also scanned on a daily basis to demonstrate that the BBB integrity was restored. The BBB returned to its original condition between days 4 and 5 (Supplementary Figure 2(a)) in three out of the four cases. The mouse that showed permanent edema also showed permanent opening.

H&E was performed in brains sonicated at 600 and 750 kPa. At these pressures, which are above the IC threshold, some of the brains showed microscopic damage. In Figure 6, microscopic images showing more obvious damage at 600 kPa are shown (at higher pressures virtually all the brains showed microscopic damage). Within the FUS-sonicated Cau-Pu (Figure 6(c)), microhemorrhages, few necrotic cells, and microvacuolations were found.

Twelve additional mice were sonicated at the same pressures with FUS in the presence of fluorescent

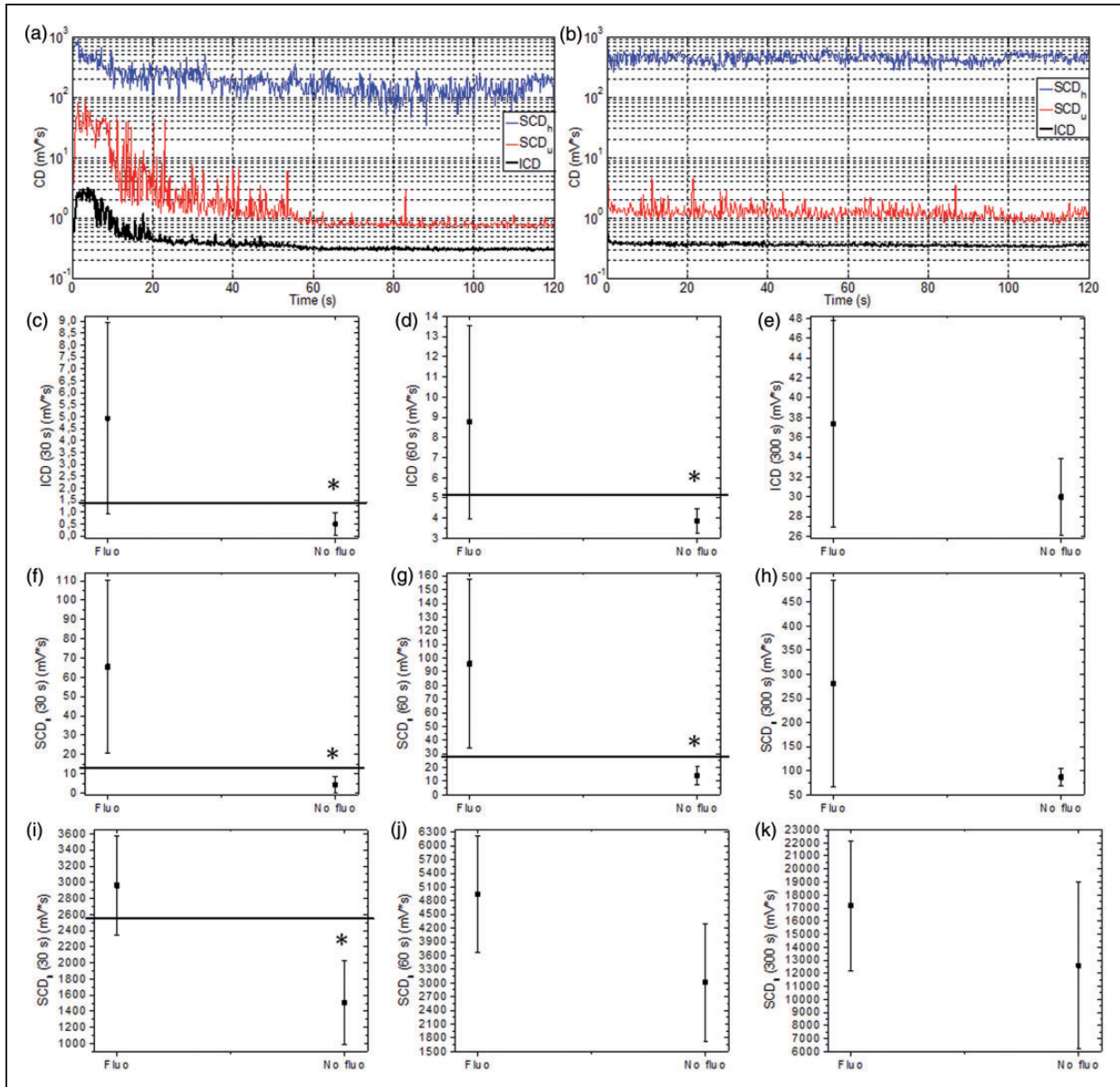


Figure 5. Cavitation doses (first 120 s) during FUS-induced BBB opening in the presence of fluorescent microbubbles for (a) a case where C-12 was successfully delivered (750 kPa) and (b) a case where C-12 was not delivered (450 kPa). Cavitation doses: ICD at (c) 30 s, (d) 1 min and (e) 5 min; SCD_u at (f) 30 s, (g) 1 min and (h) 5 min; SCD_h at (i) 30 s, (j) 1 min and (k) 5 min. Significant cavitation dose differences among cases of successful and unsuccessful C-12 delivery were found at 30 s (ICD, SCD_u, and SCD_h) and at 1 min (ICD and SCD_u), representing calculated thresholds of 1.45, 12.89, and 2,552 mV·s (at 30 s); and 5.07 and 28.09 mV·s (at 1 min). Non-significant differences were found in the rest of the cases. All numbers are reported as mean \pm sd; *: $p < 0.05$.

microbubbles and survived one week to test if damage remained or disappeared. Nine were used for H&E staining and three for Iba-1 immunohistochemistry. According to H&E staining, damage was repaired in four out of the five cases at 600 kPa, but in most (three out of the four) cases at 750 kPa, by comparing the treated with the untreated side, a higher number of cell nuclei (blue/purple color) was observed in the sonicated region compared to the unsonicated side. Figure 6 depicts the case with potential damage at 600 kPa

(Figure 6(e)) and one representative case at 750 kPa (Figure 6(g)). Three additional mice sonicated at 750 kPa and survived for one week were studied with Iba-1 bright-field immunohistochemistry in order to determine if these cell nuclei represented microglial activation (Figure 6(k)). Comparing Figure 6(i) and (k) shows that in the regions where the BBB was disrupted with FUS, although the BBB was restored (Figure 6(j)), there is microglial activation one week after treatment.

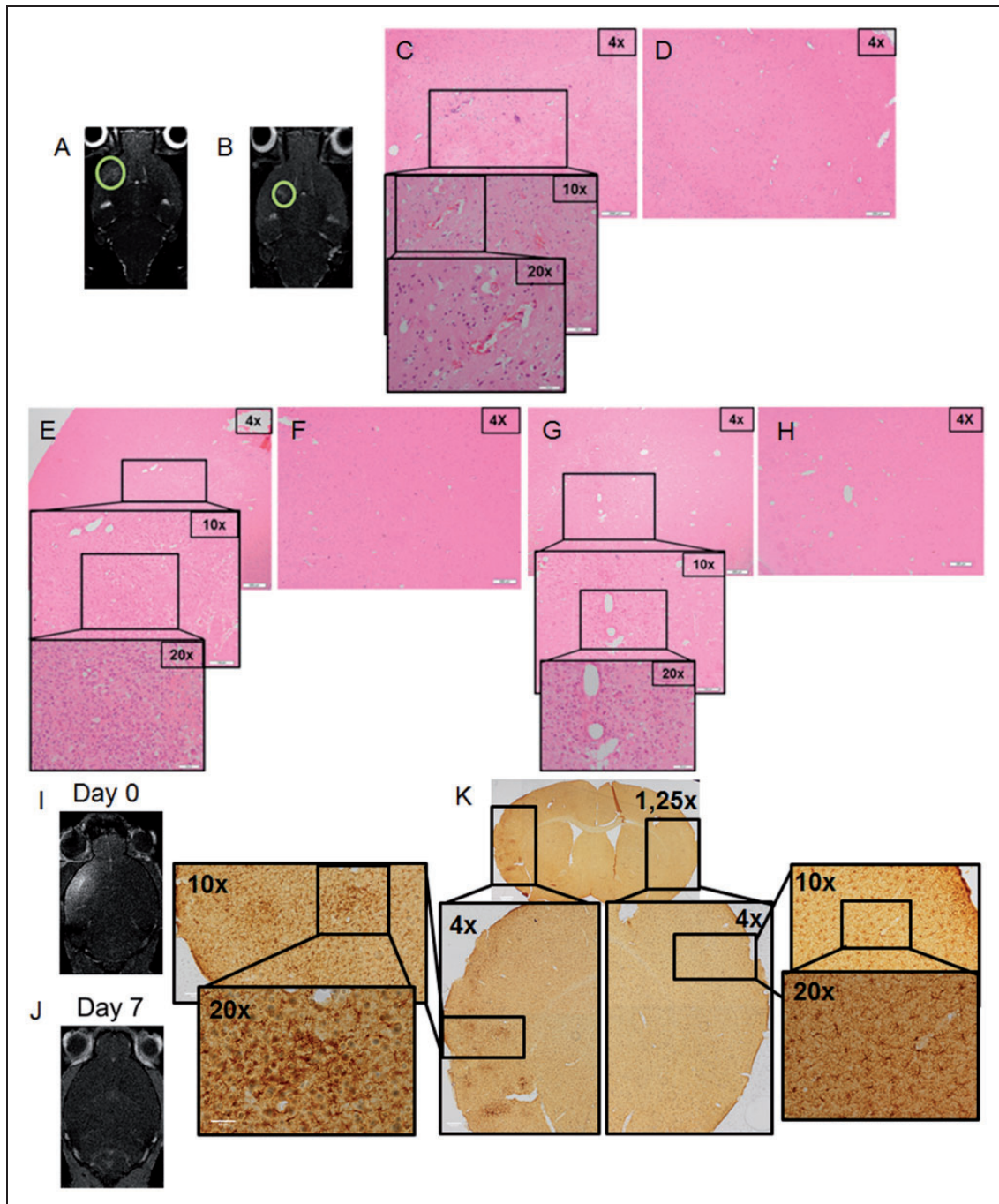


Figure 6. Safety: T₂-w MRI showing edema on day 1 (edema is usually not visible at sonication day) in the sonicated left Cau-Pu at (a) 600 kPa and (b) 750 kPa; 6- μ m-thick horizontal sections stained for H&E of mouse brains sacrificed 2 h after sonication ((c) and (d)); and sacrificed one week after sonication ((e) and (h)). (c) Left (sonicated at 600 kPa) Cau-Pu and its corresponding (d) (untreated) contralateral side. Some microhemorrhages, microvacuolations, and few necrotic cells were detected in the sonicated region (box) versus the unsonicated side which did not show damage. (e) Left (sonicated at 600 kPa) Cau-Pu and its corresponding (f) (untreated) contralateral side. Microhemorrhages were cleared out, microvacuolations disappeared, but more nuclei cells were observed in the sonicated area (box) versus the untreated contralateral side. (g) Left (sonicated at 750 kPa) Cau-Pu and its corresponding (h) (untreated) contralateral side. Same response as in (e) was observed comparing with the contralateral side. Post-contrast-enhanced T₁-w MRI showing BBB opening at day 0 (i), and BBB closing at day 7 (j) in a mouse sonicated at 750 kPa and sacrificed one week later for Iba-1 staining of 30- μ m-thick brain horizontal sections for studying microglial activation (k). Microglial activation was observed in the sonicated region (box) versus the (unsonicated) contralateral side which did not show microgliosis. The boxed regions in areas at zoom 4 \times are further zoomed in at 10 \times , while the boxed regions at zoom 10 \times are zoomed in at 20 \times . Scale bars represent 500 μ m at 1.25 \times , 200 μ m at 4 \times , 100 μ m at 10 \times and 20 μ m at 20 \times .

Discussion

Despite the significant number of studies investigating FUS-stimulated loaded microbubbles as a method for targeted drug delivery to treat different diseases, studies on drug delivery into the brain bypassing the BBB are limited and have important restrictions because they are invasive, require concurrent MRI for targeting, or lack proper safety assessment.^{16,40} All of these shortcomings have been overcome in the current study, where a new kind of lipid microbubbles was developed to serve as both a vector for targeted drug delivery and a tool for BBB opening. Departing from our conventional in-house manufactured size-selected microbubbles, the fluorophore C-12, as a model drug, was attached to the lipid shell for targeted delivery. C-12 was selected as a model drug due to two main reasons. First, its amphiphilic nature allows to significantly simplify the process of manufacturing the fluorescent microbubbles, since direct contact among the C-12 solution and the microbubbles led them towards binding to it and it was only necessary to incubate them during 2 h, at room temperature, while the syringe containing the suspension of the microbubbles loaded with C-12 was rotated at 40 r/min. For example, if the fluorescently labeled dextrans had been used, a crosslinker would have been mandatory.

The second reason lies in the fact that this fluorophore is biologically inert and therefore is safe to inject in living organisms.

In order to evaluate their feasibility for this new objective, we applied FUS in presence of the fluorescent microbubbles with the same sonication parameters used in our previous FUS-induced BBB opening experiments, and varied only the acoustic pressure, which is one of the most critical parameters determining microbubble cavitation activity. Therefore, further studies should be performed to assess how other parameters, such as frequency, pulse repetition frequency, pulse length, microbubble size, microbubble composition and microbubble stability influence the efficiency of the C-12 delivery. It is possible that the delivery of C-12 may be enhanced by customizing the aforementioned parameters.

Fluorescent microbubbles generation

As a consequence of making the monodisperse 4–5 μm microbubbles fluorescent, a decrease in their mean size of about 12% occurred. This means that we might need to apply higher pressures to achieve the same cavitation (stable and inertial) levels that in the non-fluorescent microbubbles, since the smaller the microbubbles are, the higher acoustic pressure is needed to apply them to

open the BBB.⁵⁴ However, this decrease is not deemed big enough to generate a significant effect over the cavitation levels.

The fluorescent microbubbles maintained their monodisperse distribution. There are some very large microbubbles (more than 10 μm) (Figure 1(c)), but they did not represent any safety issues. Commercial acoustic contrast agents approved by the FDA for intravascular injection, such as Sonovue, Optison, etc. contain microbubbles higher than 10 μm ; for example, Optison, although its mean diameter is 3.0–4.5 μm , contains microspheres up to 32 μm . Moreover, in our case, as it is shown in Figure 3(b), the > 10 μm concentration is negligible comparing with the microbubbles concentration in the range 2–6 μm .

BBB opening and targeted fluorophore delivery

Our fluorescent microbubbles have proven their utility as carriers of therapeutic agents in the sonicated region of the brain, concretely the left Cau-Pu in this study (successful delivery rates of 0% at 450 kPa and control conditions; 33% at 600 kPa and 60% at 750 kPa) with a successful BBB opening rate of 100% (Table 1).

Possible explanations of these successful rates are as follows. Acoustic pressures higher than 450 kPa are needed to achieve targeted delivery, so this pressure may denote the lower threshold.

Under control conditions, it means, when C-12 was co-administered freely with the microbubbles, i.e. not anchored onto their lipid shell, the delivery was unsuccessful, even at high pressures, to the sonicated region. This may be explained in terms of the amphiphilic nature of C-12. As with all the amphiphilic molecules, the C-12 presents a free lipophilic terminal, which is where the bond between the lipid shell and the fluorophore occurs. Therefore, if the C-12 is co-administered via tail vein injection, the lipophilic terminal is free and it will be trapped by lipid membranes of the endothelial cells in blood vessels and C-12 will not be able to reach the mouse brain.

Regarding 600 and 750 kPa, the successful rates may be explained by the fact that fluorescent microbubbles become quickly unstable, so the mice sonicated first, when the fluorescent microbubbles are fresher, have higher probability of showing fluorescence enhancement than mice sonicated later, when the fluorescent microbubbles are less fresh. Future studies should be performed in order to characterize the relationship between successful fluorescence delivery and freshness of the fluorescent microbubbles.

There is a relationship between the amount of C-12 delivery and the acoustic pressure; it was found that

there was a relation between 450 and 600 kPa and 450 and 750 kPa, but more studies should be done to assay if this relationship exists between 600 and 750 kPa (Figure 4(f)).

Microbubble cavitation emissions and safety evaluation

Transcranial PCD from oscillating fluorescent microbubbles has been conducted to characterize the types of cavitation during sonication in order to predict, *in vivo*, if the C-12 targeted delivery was successful or not. PCD has been used previously as a tool for predicting BBB opening, both in mice^{21,30,35,50,55,56} and in NHP.³³ In this study, transcranial PCD was utilized to define, for the first time, SCD_u , SCD_h , and ICD thresholds for successful targeted drug delivery. These thresholds are displayed in Supplementary Table 1 and were defined as twice the standard deviation above the mean of non-fluorescence (unsuccessful) delivery cavitation doses. Interestingly, these thresholds indicate that sonicating more than 2 min is not necessary to deliver C-12. This may be explained by the fact that, due to the high ICD, a significant amount of microbubbles collapsed during the first 2 min of the sonication. Therefore, during the rest of the sonication, less cavitation nuclei were available for opening the BBB and delivery the C-12. Pressures higher than 750 kPa were not tested because previous studies conducted in our laboratory showed that at higher pressures (810 kPa, 900 kPa) inertial cavitation occurs always, which might denote a successful delivery rate of 100%, but with a higher probability of microhemorrhage.^{21,54} However, other parameters, like microbubble size, composition of the lipid shell and/or gas core, pulse length, etc. will be included in future studies to evaluate and clarify the effects of SC and IC activities.

In Figure 5(a) and (b), it is observed that the success rate was probably determined by the ICD, because when it was significantly higher than zero, part of the microbubbles collapsed and C-12 was able to be delivered to the target (Figure 5(a)), but when the ICD was not significantly higher than zero, the microbubbles remained unaltered and therefore C-12 remained attached to the lipid shell, unable to cross the BBB (Figure 5(b)).

Cavitation analysis has not been carried out in previous studies of FUS-stimulated loaded microbubbles for localized drug delivery into the brain.^{16,40} These studies also may have operated in the IC regime and potentially induced microhemorrhages, although they do not report histological examinations. In this study, initial histological examinations showed microscopic damage, such as microhemorrhages, microvacuolations, and few

necrotic cells (Figure 6(c), (e) and (g)), coinciding with the high ICD needed to achieve successful C-12 delivery (Figure 5). These results were consistent with the prior findings obtained by our group,^{21,35} where the BBB opening at pressures higher than 600 kPa resulted in tissue damage at the sonicated regions. The presence of this kind of damage may compromise the safety of our technique. For this reason, nine mice were survived one week after sonication to determine whether damage was reversible. At 600 kPa, the microhemorrhage and microvacuolation were cleared, while a higher number of cell nuclei in the sonicated region compared to the same region in the contralateral side has only been observed in one out of the five cases. The same pattern appeared in three out of the four cases at 750 kPa, thereby indicating that our technique might not be safe at pressures higher than 600 kPa, at least when maintaining the rest of the sonication parameters fixed (pulse length, duration of the sonication, repetition pulse frequency) and/or the lipid and gas core composition, microbubbles size, etc. To better characterize this observation, Iba1 bright-field immunohistochemistry was performed in three additional mice sonicated at 750 kPa and survived for one week. All of them showed more microglia cells (Figure 6(k)) in the sonicated region compared to the contralateral (untreated side), it means, FUS induces, as it was shown in previous works,⁵⁷ microglial activation. Microglial activation can be really beneficial since, for example, it can reduce the burden of amyloid plaques in the brain,⁵⁷ but, it may also be harmful when it is involved in chronic neuroinflammation, it means, when the responses of microglial cells contribute to and expand the neurodestructive effects, worsening the disease process.

Therefore, another parameter to investigate is the survival duration and to increase it to two/three weeks in order to study how the microgliosis evolves.

Also, T_2 -w MRI was performed on day 1 (the day after sonication). At both pressures, edema was observed. Previous studies reported by our group have shown that edema, at acoustic pressures until 600 kPa and pulse length of 100 cycles, is cleared out over the course of a week.⁵⁴ However, in the current study some mice are sonicated at higher pressures (750 kPa), and all of them at higher pulse length (10,000 cycles). Therefore, four mice survived for two weeks after sonication at 750 kPa were scanned, on a daily basis, by T_2 -w MRI to assess whether, under the higher pressures, brain edema has been effectively repaired. In three out of the four cases, edema was repaired between days 3 and 4 (Supplementary Figure 2(b)).

These mice were also scanned, on a daily basis, by T_1 -w post-Gd injection MRI to evaluate how long it took for the BBB opening to be restored. Samiotaki

and Konofagou⁵⁸ reported that when mice were sonicated in the presence of 4–5 μm microbubbles, at a pressure of 600 kPa and pulse length of 10,000 cycles (6.7 ms), the BBB remained opened for 48–72 h, but they did not reach pressures up to 750 kPa. At this pressure, the BBB was restored between days 4 and 5 in three out of the four cases (Supplementary Figure 2(a)).

This study does present indeed certain limitations based on the success on the delivery and side-effects provoked to the high pressures used and, therefore, future work is needed to fully study the safety of our FUS technique before being applied to the clinic. These studies will be focused on evaluating the effects of using different microbubble sizes and shells (different lipids and/or different proportions), different gas cores, lower pulse lengths, lower repetition pulse frequency, reducing the sonication duration, etc. With the suitable combination of all the optimal parameters, the C-12 delivery may be achieved and enhanced at lower pressures, diminishing the side-effects provoked by the IC.

However, our findings indicate potential advantages for employing our in-house manufactured lipid microbubbles as a vector for localized drug delivery since they cause less damage than the invasive alternative methods currently used clinically for brain-targeted drug delivery, such as intracerebral-ventricular infusion,⁵⁹ convection-enhanced delivery, or implementation of delivery systems.⁶⁰ This approach, after all the parameters (acoustic pressure, pulse length, pulse repetition frequency, sonication time, lipid shell composition, microbubbles size, and gas core composition) would be optimized, might be used in humans, taking into account the differences between the thickness of the mouse ($\approx 0.2\text{ mm}$)⁵¹ and human skulls ($\approx 4.65\text{ mm}$).³³ According to our previous in vitro studies using human skulls, the FUS frequency had to be lowered to 500 kHz to decrease the aberration effects, so that SCD_h , SCD_u , and ICD were measurable.³³ Therefore, making the appropriate corrections, considering that the attenuation through the human skull is 7.33 dB/mm,³³ the method proposed herein can in principle be translated to the clinic.

Conclusion

This study evaluated the initial feasibility of FUS-induced targeted drug delivery using our in-house manufactured lipid microbubbles as a drug carrier. To this end, the lipid shell of our well characterized lipid microbubbles was loaded with the fluorophore C-12. FUS was applied in conjunction with the systemic administration of the fluorescent microbubbles and, for the first time, the existence of cavitation dose thresholds for assessing successful drug delivery was defined; for cavitation doses above these aforementioned thresholds,

significant fluorescent enhancement was observed in the sonicated left murine Cau-Pu, demonstrating targeted delivery of C-12. One week after the procedure, the BBB was closed, the edema cleared out, and only microglial activation was noticeable in some cases. Therefore, the findings presented here indicate a new safety way of FUS-induced BBB opening technology for targeted drug delivery into the brain and provide a platform for predicting successful delivery via PCD.

Funding

This work was supported in part by National Institutes of Health (R01 EB009041, R01 AG038691). Carlos Sierra additionally thanks the Alfonso Martin Escudero Foundation (Madrid, Spain) and Pedro Barrie de la Maza Foundation (A Coruña, Spain) for their funding support.

Acknowledgements

The authors would like to thank the assistance of Hoheteberhan Getachew and Oluyemi Olumade for H&E stain; and Dr. Hong Chen at the Department of Biomedical Engineering at Columbia University for insightful discussions.

Declaration of conflicting interests

The author(s) declared no potential conflicts of interest with respect to the research, authorship, and/or publication of this article.

Authors' contributions

Conception and experimental design: CS, EK, CC. Manuscript writing: CS, EK. Performing experiments: CS, CA, MK. Data analysis: CS, S-YW, MB.

Supplementary material

Supplementary material for this paper can be found at <http://jcbfm.sagepub.com/content/by/supplemental-data>

References

1. Pardridge WM. The blood-brain barrier: bottleneck in brain drug development. *NeuroRx* 2005; 2: 3–14.
2. Nutt JG, Burchiel KJ, Comella CL, et al. Randomized, double-blind trial of glial cell line-derived neurotrophic factor (GDNF) in PD. *Neurology* 2003; 60: 69–73.
3. Doolittle ND, Miner ME, Hall WA, et al. Safety and efficacy of a multicenter study using intraarterial chemotherapy in conjunction with osmotic opening of the blood-brain barrier for the treatment of patients with malignant brain tumors. *Cancer* 2000; 88: 637–647.
4. Foust KD, Nurre E, Montgomery CL, et al. Intravascular AAV9 preferentially targets neonatal neurons and adult astrocytes. *Nat Biotechnol* 2009; 27: 59–65.
5. Prades R, Oller-Salvia B, Schwarzmaier SM, et al. Applying the retro-enantio approach to obtain a peptide capable of overcoming the blood-brain barrier. *Angew Chem Int Ed Eng* 2015; 54: 3967–3972.

6. Choi JJ, Pernot M, Small SA, et al. Noninvasive, transcranial and localized opening of the blood-brain barrier using focused ultrasound in mice. *Ultrasound Med Biol* 2007; 33: 95–104.
7. Hynynen K, McDannold N, Vykhodtseva N, et al. Noninvasive MR imaging-guided focal opening of the blood-brain barrier in rabbits. *Radiology* 2001; 220: 640–646.
8. Liu HL, Wai YY, Chen WS, et al. Hemorrhage detection during focused-ultrasound induced blood-brain-barrier opening by using susceptibility-weighted magnetic resonance imaging. *Ultrasound Med Biol* 2008; 34: 598–606.
9. Yang FY, Fu WM, Yang RS, et al. Quantitative evaluation of focused ultrasound with a contrast agent on blood-brain barrier disruption. *Ultrasound Med Biol* 2007; 33: 1421–1427.
10. Choi JJ, Wang S, Brown TR, et al. Noninvasive and transient blood-brain barrier opening in the hippocampus of Alzheimer's double transgenic mice using focused ultrasound. *Ultrasonic Imag* 2008; 30: 189–200.
11. Burgess A, Huang Y, Querbes W, et al. Focused ultrasound for targeted delivery of siRNA and efficient knock-down of Htt expression. *J Control Release* 2012; 163: 125–129.
12. Baseri B, Choi JJ, Deffieux T, et al. Activation of signaling pathways following localized delivery of systemically administered neurotrophic factors across the blood-brain barrier using focused ultrasound and microbubbles. *Phys Med Biol* 2012; 57: N65–N81.
13. Samiotaki G, Acosta C, Wang S, et al. Enhanced delivery and bioactivity of the neurturin neurotrophic factor through focused ultrasound-mediated blood-brain barrier opening in vivo. *J Cereb Blood Flow Metab* 2015; 35: 600–622.
14. Wang S, Olumolade OO, Sun T, et al. Noninvasive, neuron-specific gene therapy can be facilitated by focused ultrasound and recombinant adeno-associated virus. *Gene Ther* 2015; 22: 104–110.
15. Park EJ, Zhang YZ, Vykhodtseva N, et al. Ultrasound-mediated blood-brain/blood-tumor barrier disruption improves outcomes with trastuzumab in a breast cancer brain metastasis model. *J Control Release* 163: 277–284. (201210).
16. Ting CY, Fan CH, Liu HL, et al. Concurrent blood-brain barrier opening and local drug delivery using drug-carrying microbubbles and focused ultrasound for brain glioma treatment. *Biomaterials* 2012; 33: 704–712.
17. Kovacs Z, Werner B, Rassi A, et al. Prolonged survival upon ultrasound-enhanced doxorubicin delivery in two syngenic glioblastoma mouse models. *J Control Release* 2014; 187: 74–82.
18. Alkins R, Burgess A, Ganguly M, et al. Focused ultrasound delivers targeted immune cells to metastatic brain tumors. *Cancer Res* 2013; 73: 1892–1899.
19. Fan CH, Ting CY, Chang YC, et al. Drug-loaded bubbles with matched focused ultrasound excitation for concurrent blood-brain barrier opening and brain-tumor drug delivery. *Acta Biomater* 2015; 15: 89–101.
20. Wu SK, Yang MT, Kang KH, et al. Targeted delivery of erythropoietin by transcranial focused ultrasound for neuroprotection against ischemia/reperfusion-induced neuronal injury: a long-term and short-term study. *PLoS One* 2014; 9: e90107.
21. Chen H and Konofagou EE. The size of blood-brain barrier opening induced by focused ultrasound is dictated by the acoustic pressure. *J Cereb Blood Flow Metab* 2014; 34: 1197–1204.
22. Choi JJ, Feshitan JA, Baseri B, et al. Microbubble-size dependence of focused ultrasound-induced blood-brain barrier opening in mice in vivo. *IEEE Transac Biomed Eng* 2010; 57: 145–154.
23. Samiotaki G, Vlachos F, Tung YS, et al. A quantitative pressure and microbubble-size dependence study of focused ultrasound-induced blood-brain barrier opening reversibility in vivo using MRI. *Magnet Reson Med* 2012; 67: 769–777.
24. Tung YS, Vlachos F, Feshitan JA, et al. The mechanism of interaction between focused ultrasound and microbubbles in blood-brain barrier opening in mice. *J Acoust Soc Am* 2011; 130: 3059–3067.
25. Vlachos F, Tung YS and Konofagou E. Permeability dependence study of the focused ultrasound-induced blood-brain barrier opening at distinct pressures and microbubble diameters using DCE-MRI. *Magnet Reson Med* 2011; 66: 821–830.
26. Vlachos F, Tung YS and Konofagou EE. Permeability assessment of the focused ultrasound-induced blood-brain barrier opening using dynamic contrast-enhanced MRI. *Phys Med Biol* 2010; 55: 5451–5466.
27. Wang S, Samiotaki G, Olumolade O, et al. Microbubble type and distribution dependence of focused ultrasound-induced blood-brain barrier opening. *Ultrasound Med Biol* 2014; 40: 130–137.
28. Chen H, Chen CC, Acosta C, et al. A new brain drug delivery strategy: focused ultrasound-enhanced intranasal drug delivery. *PLoS One* 2014; 9: e108880.
29. Choi JJ, Selert K, Vlachos F, et al. Noninvasive and localized neuronal delivery using short ultrasonic pulses and microbubbles. *Proc Natl Acad Sci U S A* 2011; 108: 16539–16544.
30. Tung YS, Vlachos F, Choi JJ, et al. In vivo transcranial cavitation threshold detection during ultrasound-induced blood-brain barrier opening in mice. *Phys Med Biol* 2010; 55: 6141–6155.
31. Marquet F, Teichert T, Wu SY, et al. Real-time, transcranial monitoring of safe blood-brain barrier opening in non-human primates. *PLoS One* 2014; 9: e84310.
32. Tung YS, Marquet F, Teichert T, et al. Feasibility of noninvasive cavitation-guided blood-brain barrier opening using focused ultrasound and microbubbles in nonhuman primates. *Appl Phys Lett* 2011; 98: 163704.
33. Wu SY, Tung YS, Marquet F, et al. Transcranial cavitation detection in primates during blood-brain barrier opening – a performance assessment study. *IEEE Transac Ultrason Ferroelect Freq Control* 2014; 61: 966–978.
34. Downs ME, Buch A, Sierra C, et al. Long-term safety of repeated blood-brain barrier opening via focused ultrasound with microbubbles in non-human primates performing a cognitive task. *PLoS One* 2015; 10: e0125911.

35. Chen CC, Sheeran PS, Wu SY, et al. Targeted drug delivery with focused ultrasound-induced blood-brain barrier opening using acoustically-activated nanodroplets. *J Control Release* 2013; 172: 795–804.
36. Klibanov AL, Rychak JJ, Yang WC, et al. Targeted ultrasound contrast agent for molecular imaging of inflammation in high-shear flow. *Contrast Media Mol Imag* 2006; 1: 259–266.
37. Kwekkeboom RF, Lei Z, Bogaards SJ, et al. Ultrasound and microbubble-induced local delivery of MicroRNA-based therapeutics. *Ultrasound Med Biol* 2015; 41: 163–176.
38. Phillips LC, Klibanov AL, Wamhoff BR, et al. Localized ultrasound enhances delivery of rapamycin from microbubbles to prevent smooth muscle proliferation. *J Control Release* 2011; 154: 42–49.
39. Ferrara K, Pollard R and Borden M. Ultrasound microbubble contrast agents: fundamentals and application to gene and drug delivery. *Ann Rev Biomed Eng* 2007; 9: 415–447.
40. Huang Q, Deng J, Wang F, et al. Targeted gene delivery to the mouse brain by MRI-guided focused ultrasound-induced blood-brain barrier disruption. *Exp Neurol* 2012; 233: 350–356.
41. Borden MA, Caskey CF, Little E, et al. DNA and polylysine adsorption and multilayer construction onto cationic lipid-coated microbubbles. *Langmuir* 2007; 23: 9401–9408.
42. Feshitan JA, Chen CC, Kwan JJ, et al. Microbubble size isolation by differential centrifugation. *J Colloid Interf Sci* 2009; 329: 316–324.
43. Chen CC, Wu SY, Finan JD, et al. An experimental study on the stiffness of size-isolated microbubbles using atomic force microscopy. *IEEE Transac Ultrason Ferroelect Freq Control* 2013; 60: 524–534.
44. Wu SY, Chen CC, Tung YS, et al. Effects of the microbubble shell physicochemical properties on ultrasound-mediated drug delivery to the brain. *J Control Release* 2015; 212: 30–40.
45. Burgess A and Hynynen K. Noninvasive and targeted drug delivery to the brain using focused ultrasound. *ACS Chem Neurosci* 2013; 4: 519–526.
46. Konofagou EE, Tung YS, Choi J, et al. Ultrasound-induced blood-brain barrier opening. *Curr Pharm Biotech* 2012; 13: 1332–1345.
47. Flynn HG. In: Mason WP (ed.) *Physics of acoustic cavitation in liquids*. New York: Academic, 1964, pp.58–172.
48. Leighton TG. *The acoustic bubble*. New York: Academic Press, 1994.
49. O'Reilly MA and Hynynen K. A PVDF receiver for ultrasound monitoring of transcranial focused ultrasound therapy. *IEEE Transac Biomedical Eng* 2010; 57: 2286–2294.
50. McDannold N, Vykhodtseva N and Hynynen K. Targeted disruption of the blood-brain barrier with focused ultrasound: association with cavitation activity. *Phys Med Biol* 2006; 51: 793–807.
51. Choi JJ, Pernot M, Brown TR, et al. Spatio-temporal analysis of molecular delivery through the blood-brain barrier using focused ultrasound. *Phys Med Biol* 2007; 52: 5509–5530.
52. Edelstein A, Amodaj N, Hoover K, et al. Computer control of microscopes using microManager. In: Ausubel Frederick M, et al. (eds) *Current protocols in molecular biology. Chapter 14*. Hoboken, NJ: John Wiley & Sons, Inc, 2010.
53. Choi JJ, Selert K, Gao Z, et al. Noninvasive and localized blood-brain barrier disruption using focused ultrasound can be achieved at short pulse lengths and low pulse repetition frequencies. *J Cereb Blood Flow Metab* 2011; 31: 725–737.
54. Sun T, Samiotaki G, Wang S, Acosta C, et al. Acoustic cavitation-based monitoring of the reversibility and permeability of ultrasound-induced blood-brain barrier opening. *Phys Med Biol* 2015; 60: 9079–9094.
55. McDannold N, Arvanitis CD, Vykhodtseva N, et al. Temporary disruption of the blood-brain barrier by use of ultrasound and microbubbles: safety and efficacy evaluation in rhesus macaques. *Cancer Res* 2012; 72: 3652–3663.
56. O'Reilly MA and Hynynen K. Blood-brain barrier: real-time feedback-controlled focused ultrasound disruption by using an acoustic emissions-based controller. *Radiology* 2012; 263: 96–106.
57. Leinenga G and Gotz J. Scanning ultrasound removes amyloid-beta and restores memory in an Alzheimer's disease mouse model. *Sci Transl Med* 2015; 7: 278ra33.
58. Samiotaki G and Konofagou EE. Dependence of the reversibility of focused- ultrasound-induced blood-brain barrier opening on pressure and pulse length in vivo. *IEEE Transac Ultrason Ferroelect Freq Control* 2013; 60: 2257–2265.
59. Petiet A, Santin M, Bertrand A, et al. Gadolinium-staining reveals amyloid plaques in the brain of Alzheimer's transgenic mice. *Neurobiol Aging* 2012; 33: 1533–1544.
60. Gabathuler R. Approaches to transport therapeutic drugs across the blood-brain barrier to treat brain diseases. *Neurobiol Dis* 2010; 37: 48–57.